Peiman Naseradinmousavi
Dynamic Systems and Control Laboratory,
Department of Mechanical Engineering,
San Diego State University,
San Diego, CA 92115
e-mails: pnaseradinmousavi@mail.sdsu.edu;
peiman.n.mousavi@gmail.com

Hashem Ashrafiuon
Professor
Director of Center for Nonlinear
Dynamics and Control,
Department of Mechanical Engineering,
Villanova University,
Villanova, PA 19085
e-mail: hashem.ashrafiuon@villanova.edu

Mostafa Bagheri
Dynamic Systems and Control Laboratory,
Department of Mechanical Engineering,
San Diego State University,
San Diego, CA 92115
e-mail: mbagheri@sdsu.edu

A Decentralized Neuro-Adaptive Control Scheme to Suppress Chaotic/Hyperchaotic Dynamics of Smart Valves Network

In this effort, we utilize a decentralized neuro-adaptive scheme in extinguishing both the chaotic and hyperchaotic dynamics of the so-called "Smart Valves" network. In particular, a network of two dynamically interconnected bidirectional solenoid actuated butterfly valves undergoes the harmful chaotic/hyperchaotic dynamics subject to some initial conditions and critical parameters. Crucial trade-offs, including robustness, computational burden, and practical feasibility of the control scheme, are thoroughly investigated. The advantages and shortcomings of the decentralized neuro-adaptive method are compared with those of the direct decentralized adaptive one to yield a computationally efficient, practically feasible, and robust scheme in the presence of the coupled harmful responses. [DOI: 10.1115/1.4039627]

1 Introduction

The centralized and decentralized control of large-scale networks has received considerable attention. Although the decentralized schemes have been widely employed due to their computationally efficient algorithms, but some crucial trade-offs must be carefully addressed. The critical robustness and practical feasibility aspects of the decentralized controllers, in the presence of interconnected harmful responses, need to be thoroughly investigated. Note that the decentralized control of a multiphysics electro-magneto-mechanical-fluid network would be challenging to be dealt with. Many uncertainties involved with various coupled multidisciplinary components potentially result in cumbersome computational burden in addition to the lack of robustness. Therefore, a robust, computationally efficient, and practically feasible decentralized controller is needed to be examined and then implemented in such a large-scale multi-agent network.

The so-called "smart valves" network is widely utilized in many critical infrastructures including, but not limited to, municipal piping systems, oil and gas fields, petrochemical plants, and defense industries. Such a multiphysics flow distribution network deals with various aspects of fluid mechanics, electromagnetics, and electromechanical components. The economic and even social impact of failure of such an essential network, for each application addressed previously, would be expected to be dramatic, and therefore, a robust and practically feasible control scheme is required to mitigate the effects of the harmful dynamic responses; in the presence of enormous uncertainties involved with such a large-scale network. In particular, the system we study here is a network of two dynamically interconnected bidirectional solenoid actuated butterfly valves operating in series, as shown in Fig. 1.

Note that we have previously carried out [1–16] broad analytical and experimental studies from nonlinear interconnected modeling to centralized and direct decentralized adaptive control of both an isolated actuator-valve agent and a network of two solenoid actuated butterfly valves dynamically coupled in series.

It is somewhat difficult to find specific research work related to capturing and then controlling the chaotic and hyperchaotic dynamics of smart flow distribution network using the decentralized neuro-adaptive scheme. However, some efforts can be found in Refs. [17–30] addressing the control of broad electromechanical systems. Hsiao et al. [31] studied stabilization problem for a neural-network (NN) linearly interconnected system consisting a number of NN models. They established a linear difference inclusion state-space representation for the dynamics of each NN model. Subsequently, according to the decentralized control scheme, a set of Takagi–Sugeno (T–S) fuzzy controllers was synthesized to stabilize the NN linearly interconnected system. Karpenko et al. [32] employed reinforcement learning to coordinate the motions of a pair of hydraulic actuators. Yang and Yue [33] developed an adaptive observer to reconstruct unavailable state information taking advantage of the universal approximation property of NNs. They then recursively designed an observer-based decentralized adaptive fault-tolerant control strategy by combining backstepping methods with NNs, fault-tolerant control theory, and the dynamic surface control technique. Eltantawie [34] created decentralized neuro-fuzzy controller to improve the ride comfort and increase the stability for half car suspension system using the magneto-rheological damper as a semi-active device. Shi and Singh [35] studied robust decentralized adaptive controller design for interconnected systems. They considered a general representation of interconnections when the strength of the interconnections is bounded by a pth-order polynomial in states. Duan and Min [36] solved the decentralized state-feedback control problem for a class of large-scale stochastic high-order nonlinear systems. By generalizing NN approximation approach to this kind of systems, they completely removed the growth conditions on system nonlinearities and the power order restriction. Tong et al. [37] proposed an adaptive fuzzy decentralized backstepping output feedback control to be utilized for a class of uncertain large-scale stochastic nonlinear systems without the measurements of the states. The fuzzy logic systems are used in approximating the unknown nonlinear functions, and a fuzzy state

Contributed by the Design Engineering Division of ASME for publication in the Journal of Computational and Nonlinear Dynamics. Manuscript received December 2, 2017; final manuscript received March 9, 2018; published online April 3, 2018. Assoc. Editor: Zaihua Wang.

Copyright © 2018 by ASME

Downloaded From: http://computationalnonlinear.asmedigitalcollection.asme.org/ on 04/03/2018 Terms of Use: http://www.asme.org/about-asme/terms-of-use

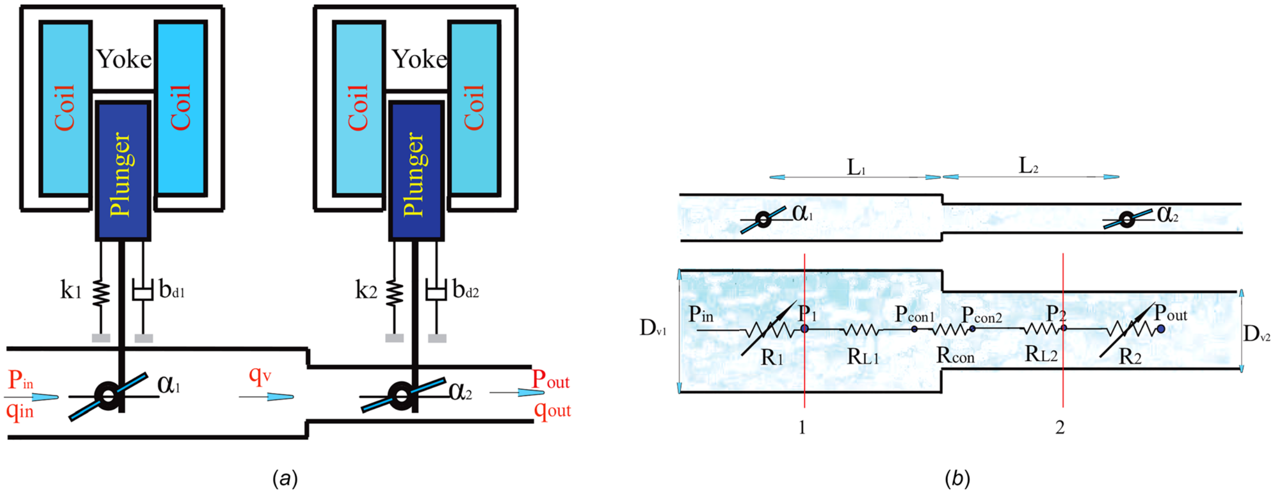

Fig. 1 (*a*) A schematic configuration of two bidirectional solenoid actuated butterfly valves subject to the sudden contraction and (*b*) a coupled model of two butterfly valves in series without actuation

observer is designed for estimating the unmeasured states. They revealed that the proposed control approach can guarantee that all the signals of the resulting closed-loop system are semi-globally uniformly ultimately bounded in probability, and the observer errors and the output of the system converge to a small neighborhood of the origin by choosing appropriate design parameters. Zhang et al. [38] investigated decentralized adaptive control for a class of discrete-time nonlinear hidden leader–follower multi-agent systems. They provided rigorous mathematical proofs to reveal that the hidden leader agent tracks the desired reference signal, all the follower agents follow the hidden leader agent, and the closed-loop system eventually achieves strong synchronization in the presence of strong couplings. Skworcow et al. [39] considered development of a methodology for an online energy and leakage management in water distribution systems, formulated within a model predictive control (MPC) framework. The approach involved calculation of control actions, i.e., time schedules for pumps, valves, and sources, to minimize the costs associated with energy used for water pumping and treatment and water losses due to leakage, while satisfying all operational constraints. Negenborn et al. [40] considered the control of large-scale transportation networks, like road traffic networks, power distribution networks, water distribution networks, etc. Control of these networks is often not possible from a single point by a single intelligent control agent; instead, control has to be performed using multiple intelligent agents. They considered multi-agent control schemes in which each agent employs a model-based predictive control approach. Coordination between the agents was used to improve decision making. Bottura and Caceres [41] analyzed river water quality systems with a serial interconnection structure with the objective of multivariable control. For the resulting block triangular system, a control design methodology was proposed in such a way to permit that from multivariable input–output data for such a type of system, both the identification by a subspace methodology previously developed be made as the corresponding decentralized control. Joseph-Duran et al. [42] presented an output-feedback control strategy for pollution mitigation in combined sewer networks. Their strategy provided means to apply model-based predictive control to large-scale sewer networks, in spite of the lack of measurements at most of the network sewers. To cope with uncertainty in system disturbances due to the stochastic water demand/consumption and optimize operational costs, Grosso et al. [43] proposed three stochastic model predictive control approaches, namely, chance-constrained MPC, tree-based MPC, and multiple-scenario MPC. Fambrini and Ocampo-Martinez [44] designed and tested MPC strategies for the global centralized and decentralized control of drinking water networks (DWN). Tests have been performed in order to highlight the advantages of having a partition of a complex network in several subsystems. Barcelli et al. [45] proposed an automatic model decomposition approach for decentralized model predictive control of DWNs. For a given DWN, the proposed algorithm partitioned the network in a set of subnetworks by taking advantage of the topology of the network, of the information about the use of actuators, and of system management heuristics.

We briefly represent the nonlinear interconnected modeling of two agents (for completeness) in addition to the initial conditions and crucial parameters resulted in the harmful dynamic responses. Then, the decentralized neuro-adaptive control scheme is formulated to be used in suppressing the interconnected chaotic and hyperchaotic dynamics of two agents. The results are thoroughly compared with those of the direct decentralized adaptive one to reveal crucial trade-offs and then yield a robust, computationally efficient, and practically feasible control scheme.

2 Mathematical Modeling

We have previously formulated [1–5] the interconnected analytical model of two agents operating in series and briefly represent here for completeness. The small-scale network being studied here is a set of two symmetric butterfly valves driven by bidirectional solenoid actuators (Fig. 1) through rack and pinion arrangements. Note that utilizing the rack and pinion mechanism provides the kinematic constraint helping us to formulate the coupled multiphysics model of two agents.

Developing such an interconnected multiphysics model undoubtedly needs some simplifying assumptions to be applied. Among those assumptions reported earlier [1–5], the most important one is to assume the dominant laminar flow for both the coupled valves in order to avoid the numerical difficulties involved with a turbulent regime. However, a critical issue needs to be addressed with respect to the validity of such an assumption. The values of pipe diameters and flow mean velocity given in Table 1 expectedly indicate the existence of the turbulent regime invalidating the assumption we have made. From another aspect, the analytical formulas of the flow loads, including the hydrodynamic and bearing torques, were formulated based on the assumption of laminar flow [46]. To address the issues discussed previously, we have carried out experimental work [47], shown in Fig. 2, to measure the sum of the hydrodynamic and bearing torques as the most affecting loads on the valves and subsequently, the dynamics of the actuators. The experiment yielded the total torque for the inlet velocity of $v \approx 2.7(\mathrm{m/s})$ and valve diameter of $D_v = 2$ in reasonably validating the laminar flow assumption.

Downloaded From: http://computationalnonlinear.asmedigitalcollection.asme.org/ on 04/03/2018 Terms of Use: http://www.asme.org/about-asme/terms-of-use

Table 1 The system parameters

ρ	$1000\ (\mathrm{kg/m^3})$	v	$3\ (\mathrm{m/s})$
$J_{1,2}$	$0.104\times10^{-1}\ (\mathrm{kg\ m^2})$	N_2	3300
N_1	3300	$C_{11,22}$	$1.56\times10^{6}\ (H^{-1})$
D_{v1}	0.2032 (m)	D_{v2}	0.127 (m)
$D_{s1,s2}$	0.01 (m)	P_{out}	2 (kPa)
$k_{1,2}$	$60\ (\mathrm{N{\cdot}m^{-1}})$	$C_{21,22}$	$6.32\times10^{8}\ (H^{-1})$
L_1	2 (m)	L_2	1 (m)
$r_{1,2}$	0.05 (m)	θ	90 deg
P_{in}	256 (kPa)	$g_{m1,m2}$	0.1 (m)
μ_f	$0.018\ (\mathrm{kg\ m^{-1}\ s^{-1}})$	$b_{di}=\mu_i$	1×10^{-7}
$\varepsilon_{1,2}$	5×10^{-3}		

We proposed an effective method of "coupled resistances" [1–5] to model the interconnected agents by utilizing the mass continuity and postdiffusion electromagnetic principles. Note that the inlet and outlet pressures were supposed to be known. As can be observed in Fig. 1(*b*), the valves are modeled as changing resistors

$$R_{ni}(\alpha_i)=\frac{e_i}{\left(p_i\alpha_i^3+q_i\alpha_i^2+o_i\alpha_i+\gamma_i\right)^2},\quad (i=1,2) \tag{1}$$

where, R_{n1} and R_{n2} indicate the resistances of the upstream and downstream valves, respectively, and $e_1=7.2\times10^5$, $p_1=461.9$, $q_1=-405.4$, $o_1=-1831$, $\gamma_1=2207$, $e_2=4.51\times10^5$, $p_2=161.84$, $q_2=-110.53$, $o_2=-695.1$, and $\gamma_2=807.57$ for two different valves' diameters. Also, the flow between the valves in addition to the sudden contraction is modeled as constant resistors based on the Hagen–Poiseuille and Borda–Carnot formulas [48,49]

$$R_{Li}=\frac{128\mu_f L_i}{\pi D_{vi}^4},\quad (i=1,2) \tag{2}$$

$$R_{\mathrm{con}}=\frac{8K_{\mathrm{con}}}{\pi^2 D_{v2}^4} \tag{3}$$

where $K_{\mathrm{con}}=0.5(1-\beta^2)\sqrt{\sin(\theta/2)}$, β indicates the ratio of minor and major diameters (D_{v2}/D_{v1}), θ is the angle of approach (the pipe contraction angle), μ_f stands for the fluid dynamic viscosity, D_{v1} and D_{v2} are the upstream and downstream valves' diameters, respectively, L_1 and L_2 indicate the pipe lengths before and after contraction, and R_{L1} and R_{L2} are the constant resistances. Therefore, two valves operating in series can be modeled as a set of five resistors, leading us to derive mathematical expressions of the pressures after and before the upstream and downstream valves, respectively, as follows [1–5]:

$$P_1=\frac{R_{n2}P_{\mathrm{in}}+R_{n1}P_{\mathrm{out}}+R_{n1}(R_{L1}+R_{L2}+R_{\mathrm{con}}q_v)q_v}{(R_{n1}+R_{n2})} \tag{4}$$

$$P_2=\frac{R_{n2}P_{\mathrm{in}}+R_{n1}P_{\mathrm{out}}-R_{n2}(R_{L1}+R_{L2}+R_{\mathrm{con}}q_v)q_v}{(R_{n1}+R_{n2})} \tag{5}$$

where q_v is the volumetric flow rate. These interconnected pressures were used in developing both the coupled hydrodynamic and bearing torques [1–5]

$$\begin{aligned}T_{h1}&=\left(a_1\alpha_1 e^{b_1\alpha_1^{1.1}}-c_1 e^{d_1\alpha_1}\right)(P_{\mathrm{in}}-P_1)\\&=\left(a_1\alpha_1 e^{b_1\alpha_1^{1.1}}-c_1 e^{d_1\alpha_1}\right)\times\frac{\dfrac{e_1}{\left(p_1\alpha_1^3+q_1\alpha_1^2+o_1\alpha_1+\gamma_1\right)^2}}{\displaystyle\sum_{i=1}^{2}\frac{e_i}{\left(p_i\alpha_i^3+q_i\alpha_i^2+o_i\alpha_i+\gamma_i\right)^2}}\\&\quad\times\left(P_{\mathrm{in}}-P_{\mathrm{out}}-(R_{L1}+R_{L2}+R_{\mathrm{con}}q_v)q_v\right)\end{aligned} \tag{6}$$

$$\begin{aligned}T_{h2}&=\left(a_1'\alpha_2 e^{b_1'\alpha_2^{1.1}}-c_1' e^{d_1'\alpha_2}\right)(P_2-P_{\mathrm{out}})\\&=\left(a_1'\alpha_2 e^{b_1'\alpha_2^{1.1}}-c_1' e^{d_1'\alpha_2}\right)\times\frac{\dfrac{e_2}{\left(p_2\alpha_2^3+q_2\alpha_2^2+o_2\alpha_2+\gamma_2\right)^2}}{\displaystyle\sum_{i=1}^{2}\frac{e_i}{\left(p_i\alpha_i^3+q_i\alpha_i^2+o_i\alpha_i+\gamma_i\right)^2}}\\&\quad\times\left(P_{\mathrm{in}}-P_{\mathrm{out}}-(R_{L1}+R_{L2}+R_{\mathrm{con}}q_v)q_v\right)\end{aligned} \tag{7}$$

$$T_{b1}=C_1\Delta P_1(R_{n1},R_{n2},R_{L1},R_{L2},R_{\mathrm{con}}) \tag{8}$$

$$T_{b2}=C_2\Delta P_2(R_{n1},R_{n2},R_{L1},R_{L2},R_{\mathrm{con}}) \tag{9}$$

where $a_1=0.4249$, $a_1'=0.1022$, $b_1=-18.52$, $b_1'=-17.0795$, $c_1=-7.823\times10^{-4}$, $c_1'=-2\times10^{-4}$, $d_1=-1.084$, $d_1'=-1.0973$, $C_1=C_2=0.5A_d\mu D_s$, $\Delta P_1=P_{\mathrm{in}}-P_1$, $\Delta P_2=P_2-P_{\mathrm{out}}$, and P_{in} and P_{out} are the inlet and outlet pressures given, respectively. Note that D_s is the stem diameter of the valve and μ stands for the friction coefficient of the bearing area. We have previously established that the hydrodynamic torque acts as a helping load pushing the valve to be closed and is typically effective for when the valve angle is lower than 60 deg [1–16]; the effective range was experimentally examined [47] confirming the helping behavior of the hydrodynamic torque by presenting positive values. The bearing torque, due to its friction-based nature, always acts as a resisting load. Using these tools, we could formulate the sixth-order interconnected model of two agents as follows:

$$\dot z_1=z_2 \tag{10}$$

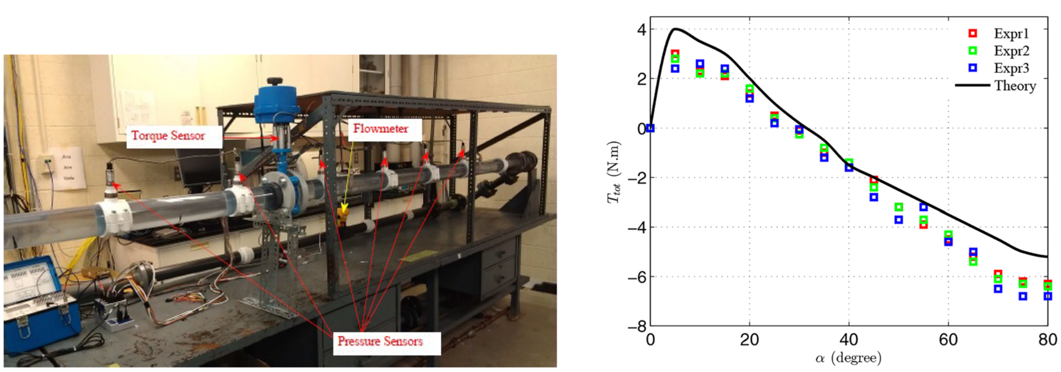

(*a*) (*b*)

Fig. 2 (*a*) The experimental work setup and (*b*) the experimentally measured total flow loads

Downloaded From: http://computationalnonlinear.asmedigitalcollection.asme.org/ on 04/03/2018 Terms of Use: http://www.asme.org/about-asme/terms-of-use

$$\dot{z}_2=\frac{1}{J_1}\left[\frac{r_1C_{21}N_1^2z_3^2}{2\left(C_{11}+C_{21}(g_{m1}-r_1z_1)\right)^2}-b_{d1}z_2-k_1z_1+\frac{\dfrac{(P_{\text{in}}-P_{\text{out}}-(R_{L1}+R_{L2}+R_{\text{con}}q_v)q_v)e_1}{\left(p_1z_1^3+q_1z_1^2+o_1z_1+\gamma_1\right)^2}}{\sum\limits_{i=1,4}\dfrac{e_i}{\left(p_iz_i^3+q_iz_i^2+o_iz_i+\gamma_i\right)^2}}\times\left[\left(a_1z_1e^{b_1z_1^{1.1}}-c_1e^{d_1z_1}\right)-C_1\times\tanh(Kz_2)\right]\right] \tag{11}$$

$$\dot{z}_3=\frac{\left(V_1-R_1z_3\right)\left(C_{11}+C_{21}(g_{m1}-r_1z_1)\right)}{N_1^2}-\frac{r_1C_{21}z_3z_2}{\left(C_{11}+C_{21}(g_{m1}-r_1z_1)\right)} \tag{12}$$

$$\dot{z}_4=z_5 \tag{13}$$

$$\dot{z}_5=\frac{1}{J_2}\left[\frac{r_2C_{22}N_2^2z_6^2}{2\left(C_{12}+C_{22}(g_{m2}-r_2z_4)\right)^2}-b_{d2}z_5-k_2z_4+\frac{\dfrac{(P_{\text{in}}-P_{\text{out}}-(R_{L1}+R_{L2}+R_{\text{con}}q_v)q_v)e_2}{\left(p_2z_4^3+q_2z_4^2+o_2z_4+\gamma_2\right)^2}}{\sum\limits_{i=1,4}\dfrac{e_i}{\left(p_iz_i^3+q_iz_i^2+o_iz_i+\gamma_i\right)^2}}\times\left[\left(a_1'z_4e^{b_1'z_4^{1.1}}-c_1'e^{d_1'z_4}\right)-C_2\times\tanh(Kz_5)\right]\right] \tag{14}$$

$$\dot{z}_6=\frac{\left(V_2-R_2z_6\right)\left(C_{12}+C_{22}(g_{m2}-r_2z_4)\right)}{N_2^2}-\frac{r_2C_{22}z_5z_6}{\left(C_{12}+C_{22}(g_{m2}-r_2z_4)\right)} \tag{15}$$

where, b_{di} indicates the equivalent torsional damping, k_i is the equivalent torsional stiffness, V_i stands for the supply voltage, r_i indicates the radius of the pinion, C_{1i} and C_{2i} are the reluctances of the magnetic path without air gap and that of the air gap, respectively, N_i stands for the number of coils, g_{mi} is the nominal air gap, J_i indicates the polar moment of inertia of the valve's disk, and R_i is the electrical resistance of coil. $z_1=\alpha_1$, $z_2=\dot{\alpha}_1$, and $z_3=i_1$ indicate the upstream valve's rotation angle, angular velocity, and actuator current, respectively. $z_4=\alpha_2$, $z_5=\dot{\alpha}_2$, and $z_6=i_2$ stand for the downstream valve's rotation angle, angular velocity, and actuator current, respectively. The network parameters are listed in Table 1. Note that it is important to thoroughly study the existence and uniqueness of solution of the model formulated. Equations (10)–(15) can be lumped as

$$\dot{Z}=F(Z) \tag{16}$$

where $Z=[z_1,z_2,z_3,z_4,z_5,z_6]^{\mathrm{T}}$.

THEOREM 1. *Assume F(Z) is a continuous function [50] in a region given as*

$$R=\{Z\in\Re^n:||Z-Z_0||\le a\},\quad a>0 \tag{17}$$

Since F is continuous in a closed and bounded domain, it is necessarily bounded in R:

$$\exists K>0\quad\text{such that}\quad ||F(Z)||\le K\quad\forall Z\in R \tag{18}$$

Based on the theorem, it is straightforward to conclude that $\dot{Z}=F(Z)$ has at least one solution.

THEOREM 2. *Assume F and $\partial F/\partial Z$ are continuous functions in R [50] defined through the existence theorem. Therefore, both the F and $\partial F/\partial Z$ are bounded in R whereas F is Lipschitz:*

$$\begin{aligned}&\exists K,L>0\quad\text{such that}\quad ||F(Z)||\le K\quad\text{and}\\&||F(Z)-F(Y)||\le L||Z-Y||\quad\forall Z,Y\in R\end{aligned} \tag{19}$$

This indicates that $\dot{Z}=F(Z)$ has at most one solution.

Comparing the conclusion of at most one solution with the existence theorem leads to a unique solution of $\dot{Z}=F(Z)$. It is obvious that all F_ϕ's and $(\partial F_\phi/\partial z_\psi)(\phi,\psi=1,\ldots,6)$ are continuous on a certain operational domain (open and connected set, $D\subset\Re^6$) of the system; there is no singular point in the operational domain. Consequently, F_ϕ's and $\partial F_\phi/\partial z_\psi$ are bounded in D resulting in a Lipschitz F at every point $z\in D$.

By exposing the coupled agents to the critical parameters of $b_{di}=\mu_i=1\times10^{-7}$ along with a set of certain initial conditions, we could capture [2], for the first time, the interconnected chaotic and hyperchaotic dynamics shown in Figs. 3(*a*) and 3(*b*), respectively. The initial conditions leading to the coupled chaos and hyperchaos are initial$_1$ = [20(deg) 0 0 20(deg) 0 0] and initial$_2$ = [2(deg) 0 0 2(deg) 0 0], respectively. We utilized the powerful tools of Lyapunov exponents and Poincaré map to distinguish between the responses. The Lyapunov exponent is a powerful indicator to reveal the divergence rate of two nearby trajectories (valves-actuators)

$$L_j=\lim_{t\to\infty|\Delta\mathbf{z}_{j0}|\to0}\frac{1}{t}\ln\frac{|\Delta\mathbf{z}_j(\mathbf{z}_{j0},t)|}{|\Delta\mathbf{z}_{j0}|} \tag{20}$$

Downloaded From: http://computationalnonlinear.asmedigitalcollection.asme.org/ on 04/03/2018 Terms of Use: http://www.asme.org/about-asme/terms-of-use

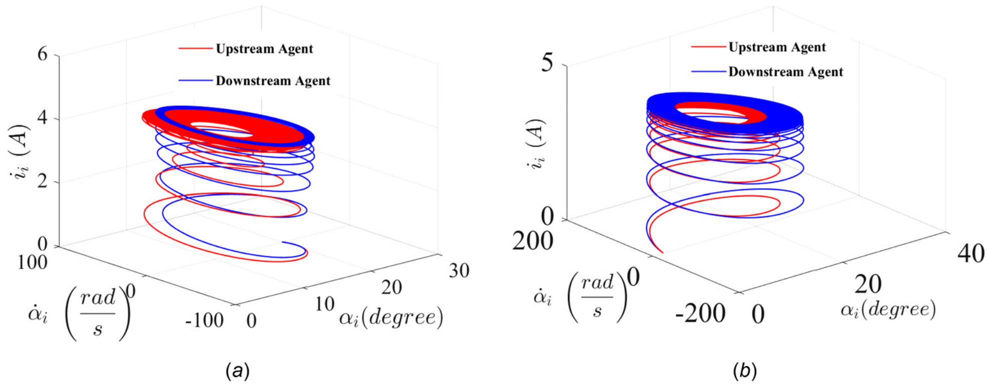

Fig. 3 (*a*) The coupled sets' phase portraits for initial$_1$ and (*b*) the coupled sets' phase portraits for initial$_2$

The algorithm utilized in determining Lyapunov exponents can be found in Ref. [51]. One and two positive Lyapunov exponents shown in Figs. 4(*a*) and 4(*b*) indicate the chaotic and hyperchaotic dynamics of the two agents. The irregular Poincaré maps (Figs. 4(*c*)–4(*f*)) confirm the existence of the harmful responses.

Extinguishing such harmful dynamic responses, in particular with larger domains of attractions, would undoubtedly require a robust, computationally efficient, and more importantly, practically feasible control scheme. We have previously examined a centralized adaptive method [1] by yielding practically feasible control inputs although with a considerable computation time. The issue of computational burden, particularly for the large-scale networks, led us to examine the direct decentralized adaptive method [11]. The decentralized scheme's computation time was one-sixtieth of the centralized one although yielded practically infeasible control inputs. Therefore, we here examine a decentralized combinatorial method to possibly fix the shortcomings of the direct decentralized adaptive one.

3 Decentralized Neuro-Adaptive Scheme

The decentralized neuro-adaptive scheme reported in Refs. [52–55] is utilized for tracking energy-efficient trajectories [3,4] defined based on the crucial initial conditions

$$\alpha_{di} = \frac{\pi}{3}\tanh(10^{-4}t^3) + \frac{\pi}{9},\ \text{Initial}_1 \tag{21}$$

$$\alpha_{di} = \frac{\pi}{3}\tanh(10^{-4}t^3) + \frac{\pi}{90},\ \text{Initial}_2 \tag{22}$$

Note that the so-called "S-Shaped" trajectories are highly energy-efficient [4] and yield smooth dynamic responses avoiding the repeatedly observed dangerous phenomenon of "Water Hammering." We rewrite the interconnected dynamic Eqs. (11) and (14) as

$$J_i\ddot{\alpha}_i + b_{di}\dot{\alpha}_i + k_i\alpha_i = \frac{r_i C_{2i} N_i^2 u_i}{2\big(C_{1i} + C_{2i}(g_{mi} - r_i\alpha_i)\big)^2} + \frac{A_1 R_{ni}}{\sum_{i=1}^{2} R_{ni}} \times \left[T'_{hi} - T'_{bi}\tanh(K\dot{\alpha}_i)\right], \quad (i = 1, 2) \tag{23}$$

where $A_1 = (P_{\text{in}} - P_{\text{out}} - (R_{L1} + R_{L2} + R_{\text{con}} q_v) q_v)$, $T'_{h1} = a_1\alpha_1 e^{b_1\alpha_1^{1.1}} - c_1 e^{d_1\alpha_1}$, $T'_{h2} = a'_1\alpha_2 e^{b'_1\alpha_2^{1.1}} - c'_1 e^{d'_1\alpha_2}$, and $T'_{bi} = 0.5A_{di}\mu_i D_{si}$.

Generally, a large-scale network containing N interconnected agents, here $N = 2$, can be expressed as follows:

$$\dot{x}_{i,1} = x_{i,2} \tag{24}$$

$$\dot{x}_{i,n_i} = f_i(\mathbf{x}_i, u_i) + \Delta_i(\mathbf{x}_1, \mathbf{x}_2, \ldots, \mathbf{x}_N) \tag{25}$$

$$y_i = x_{i,1} \tag{26}$$

where $\mathbf{x}_i = [x_{i,1}, x_{i,2}, \ldots, x_{i,n_i}]^{\mathrm{T}}$ is the state vector of ith agent and $\mathbf{x} = [\mathbf{x}_1^{\mathrm{T}}, \mathbf{x}_2^{\mathrm{T}}, \ldots, \mathbf{x}_N^{\mathrm{T}}]^{\mathrm{T}}$ indicates the full state of the whole network. u_i and y_i stand for the decentralized input and output of the ith agent, respectively; $f_i(\mathbf{x}_i, u_i)$ is a smooth function and $|\Delta_i(\mathbf{x}_1, \mathbf{x}_1, \ldots, \mathbf{x}_N)| \le \varepsilon_i\ (\varepsilon_i > 0)$ stands for the effects of the other interconnected sets.

By defining the tracking error $e_i = \underbrace{y_i}_{\alpha_i} - \underbrace{r_{di}}_{\alpha_{di}}$, the error vector of the ith agent is written as $\mathbf{e}_i = [e_i, \dot{e}_i, \ldots, e_i^{(n_i-1)}]^{\mathrm{T}}$ with the time derivative of $\dot{\mathbf{e}}_\mathbf{i} = [\dot{e}_i, e_i^{(2)}, \ldots, e_i^{(n_i)}]^{\mathrm{T}}$, $(i = 1, 2)$.

The error dynamics can be therefore written as

$$e_i^{(n_i)} = y_i^{(n_i)} - r_{di}^{(n_i)} \tag{27}$$

$$= \dot{x}_{i,n_i} - r_{di}^{(n_i)} \tag{28}$$

$$= f_i(\mathbf{x}_i, u_i) + \Delta_i(\mathbf{x}_1, \mathbf{x}_2, \ldots, \mathbf{x}_N) - r_{di}^{(n_i)} \tag{29}$$

Using the mean value theorem [56], we have

$$f_i(\mathbf{x}_i, u_i) = f_i(\mathbf{x}_i, u_i^*) + (u_i - u_i^*) f_{u_i} \tag{30}$$

where $f_{u_i} = (\partial f_i(\mathbf{x}_i, u_i)/\partial u_i)_{|u_i = u_{\lambda_i}}$, $\lambda \in (0, 1)$, and $u_{\lambda_i} = \lambda_i u_i + (1 - \lambda_i) u_i^*$. Substituting Eq. (30) into Eq. (29) yields

$$e_i^{(n_i)} = f_i(\mathbf{x}_i, u_i^*) + (u_i - u_i^*) f_{u_i} + \Delta_i - r_{di}^{(n_i)} \tag{31}$$

Assuming $v_i = f_i(\mathbf{x}_i, u_i^*)$, which is a pseudocontrol signal, and rewriting Eq. (31) give

$$e_i^{(n_i)} = v_i + (u_i - u_i^*) f_{u_i} + \Delta_i - r_{di}^{(n_i)} \tag{32}$$

Hence, the pseudocontrol v_i [52] is derived as

$$v_i = -(a_{i,n_i-1} e_i^{(n_i-1)} + \cdots + a_{i,1}\dot{e}_i + a_{i,0} e_i) + r_{di}^{(n_i)} \tag{33}$$

The coefficients of error terms are selected such that $L_i(s) = s^{(n_i)} + a_{i,n_i-1} s^{(n_i-1)} + \cdots + a_{i,0}$ becomes Hurwitz. Substituting Eq. (33) into Eq. (32) yields

$$e_i^{(n_i)} = -(a_{i,n_i-1} e_i^{(n_i-1)} + \cdots + a_{i,1}\dot{e}_i + a_{i,0} e_i) + (u_i - u_i^*) f_{u_i} + \Delta_i \tag{34}$$

Downloaded From: http://computationalnonlinear.asmedigitalcollection.asme.org/ on 04/03/2018 Terms of Use: http://www.asme.org/about-asme/terms-of-use

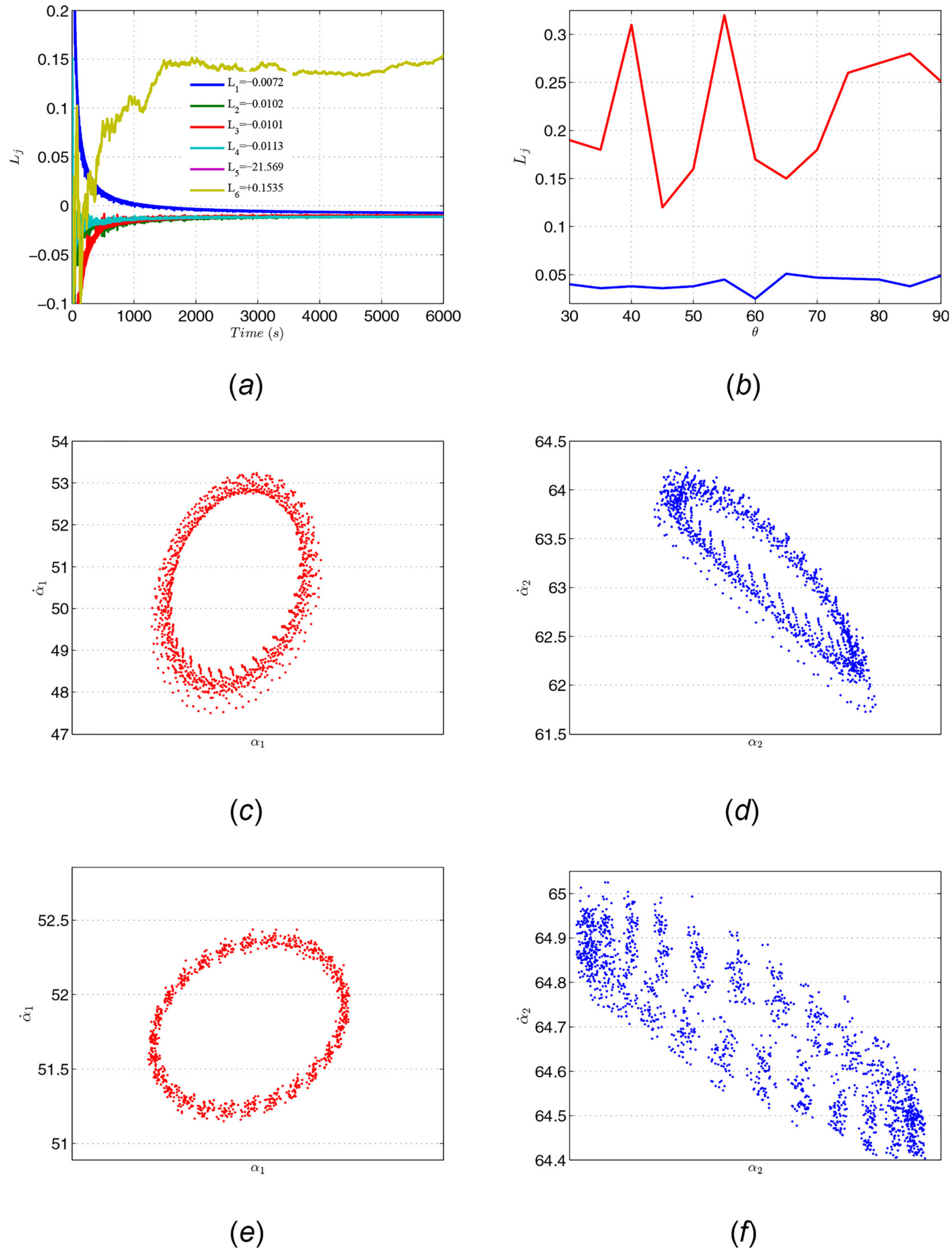

Fig. 4 **(*a*) The Lyapunov exponents for initial$_1$, (*b*) the positive Lyapunov exponents for initial$_2$ versus different approach angles (θ), (*c*) the Poincaré map for initial$_1$ of the upstream set, (*d*) the Poincaré map for initial$_1$ of the downstream set, (*e*) the Poincaré map for initial$_2$ of the upstream set, and (*f*) the Poincaré map for initial$_2$ of the downstream set**

Therefore, the error dynamics can be expressed as follows:

$$\dot{\mathbf{e}}_\mathbf{i} = \mathbf{A}_\mathbf{i}\mathbf{e}_\mathbf{i} + \mathbf{b}_i((u_i - u_i^*)f_{u_i} + \Delta_i), \quad (i = 1, 2) \tag{35}$$

The matrix $\mathbf{A_i}$ is Hurwitz and $\mathbf{b}_i = [0\,1]^{\mathrm{T}}$ for the two interconnected agents subject to the chaotic and hyperchaotic dynamics. The Hurwitz $\mathbf{A_i}$ leads to a unique positive definite P_i to be calculated through the Lyapunov equation

$$A_i^{\mathrm{T}} P_i + P_i A_i = -Q_i \tag{36}$$

where Q_i is a positive definite matrix.

The following decentralized neuro-adaptive control inputs developed in Ref. [52] are utilized in extinguishing the harmful responses:

$$\begin{aligned} u_{dni} = {} & \hat{B}_i^{\mathrm{T}} \psi_{b_i}(\mathbf{z}_i) - \left(\mathbf{e}_i^{\mathrm{T}} P_i \mathbf{b}_i\right) \hat{C}_i^{\mathrm{T}} \psi_{c_i}\left(\mathbf{e}_i^{\mathrm{T}} P_i \mathbf{b}_i\right) - \hat{\zeta}_i \mathrm{sgn}\left(\mathbf{e}_i^{\mathrm{T}} P_i \mathbf{b}_i\right) \\ & - \left(\mathbf{e}_i^{\mathrm{T}} P_i \mathbf{b}_i\right) \hat{\Omega}_i + u_{i,k}(\mathbf{z}_i) - \frac{N\left(\mathbf{e}_i^{\mathrm{T}} P_i \mathbf{b}_i\right)}{2\left(f_i^L\right)^2}, \quad (i = 1, 2) \end{aligned} \tag{37}$$

where $\hat{B}_i^{\mathrm{T}} \psi_{b_i}(\mathbf{z}_i)$ indicates the radial basis neural network employed to approximate the ideal controller for the network,

Downloaded From: http://computationalnonlinear.asmedigitalcollection.asme.org/ on 04/03/2018 Terms of Use: http://www.asme.org/about-asme/terms-of-use

$\mathbf{z}_i = [\mathbf{x}_i^{\mathrm{T}}, v_i]^{\mathrm{T}}$, $\psi_{b_i}(\mathbf{z}_i) \in \Re^{K_i}$ stands for the NN basis vector, K_i is the NN's number of nodes, the second term $(\mathbf{e}_i^{\mathrm{T}} P_i \mathbf{b}_i)\hat{C}_i^{\mathrm{T}} \psi_{c_i}(\mathbf{e}_i^{\mathrm{T}} P_i \mathbf{b}_i)$ is utilized in compensating for the interconnections' nonlinearities, the $u_{i,k}(\mathbf{z}_i)$ stands for a prior continuous controller designed in advanced via heuristics or past experiences with the application of conventional control methods, and $\hat{\zeta}_i \mathrm{sgn}(\mathbf{e}_i^{\mathrm{T}} P_i \mathbf{b}_i)$, $(\mathbf{e}_i^{\mathrm{T}} P_i \mathbf{b}_i)\hat{\Omega}_i$, and $(N(\mathbf{e}_i^{\mathrm{T}} P_i \mathbf{b}_i)/2(f_i^L)^2)$ are used in dealing with uncertainties in the neural network approximation error and the network interconnections.

Also, the following neuro-based adaptation laws are employed:

$$\dot{\hat{B}}_i = -\Gamma_{b_i} \mathbf{e}_i^{\mathrm{T}} P_i \mathbf{b}_i \psi_{b_i}(\mathbf{z}_i) \tag{38}$$

$$\dot{\hat{C}}_i = \Gamma_{c_i} (\mathbf{e}_i^{\mathrm{T}} P_i \mathbf{b}_i)^2 \psi_{c_i}(\mathbf{e}_i^{\mathrm{T}} P_i \mathbf{b}_i) \tag{39}$$

$$\dot{\hat{\zeta}}_i = \gamma_{\zeta_i} |\mathbf{e}_i^{\mathrm{T}} P_i \mathbf{b}_i| \tag{40}$$

$$\dot{\hat{\Omega}}_i = \gamma_{\Omega_i} (\mathbf{e}_i^{\mathrm{T}} P_i \mathbf{b}_i)^2 \tag{41}$$

where Γ_{b_i}, Γ_{c_i}, γ_{ζ_i}, and γ_{Ω_i} are constant adaptation gains. Note that the decentralized neuro-adaptive control and adaptation laws developed in Ref. [57] guarantee asymptotic convergence of the tracking errors to zero and also boundedness of the closed-loop network using Barbalat and the following lemmas and assumption.

Assumption. *For each agent, the followings are valid for positive constants f_i^L and H_i:*

$$0 < f_i^L \le \frac{\partial f_i(\mathbf{x}_i, u_i)}{\partial u_i} \tag{42}$$

$$\left| \frac{d}{dt} \left[\frac{\partial f_i(\mathbf{x}_i, u_i)}{\partial u_i} \right] \right| \le H_i < \frac{\lambda_{\min}(Q_i)}{\lambda_{\max}(P_i)} f_i^L \tag{43}$$

where Q_i and P_i are the positive-definite matrices.

Lemma. *For the ith agent described in Eqs. (24)–(26) satisfying the above-mentioned assumption and also other conditions given in Ref. [58], the following inequality is valid:*

$$\frac{e_i^{\mathrm{T}} Q_i e_i}{2 f_{u_i}} + \frac{e_i^{\mathrm{T}} P_i e_i \dot{f}_{u_i}}{2 f_{u_i}^2} \ge 0 \tag{44}$$

Therefore, by selecting the Lyapunov function as

$$V = \sum_{i=1}^{N} \frac{e_i^{\mathrm{T}} P_i e_i}{2 f_{u_i}} + \frac{1}{2} \left[\tilde{B}_i^{\mathrm{T}} \Gamma_{b_i}^{-1} \tilde{B}_i + \tilde{C}_i^{\mathrm{T}} \Gamma_{c_i}^{-1} \tilde{C}_i + \frac{\tilde{\zeta}_i^2}{\gamma_{\zeta_i}} + \frac{\tilde{\Omega}_i^2}{\gamma_{\Omega_i}} \right] \tag{45}$$

One can obtain $\dot{V}$ as follows:

$$\dot{V} \le -\sum_{i=1}^{N} \left[\frac{e_i^{\mathrm{T}} Q_i e_i}{2 f_{u_i}} + \frac{e_i^{\mathrm{T}} P_i e_i \dot{f}_{u_i}}{2 f_{u_i}^2} \right] \tag{46}$$

The $\dot{V}$ indicates asymptotic converge of the tracking errors to zero, based on the lemma mentioned, in addition to the boundedness of the closed-loop network. Note that we have previously utilized the direct decentralized adaptive scheme [11] using the following control and adaptation laws:

$$u_{ddi} = \frac{\nu_i}{\hat{\eta}_i} \tag{47}$$

$$\nu_i = \left(a_{i,0} e_i + a_{i,1} \dot{e}_i + a_{i,2} e_i^{(2)} + \cdots + a_{i,n_i-1} e_i^{(n_i-1)} \right) - \sum_{w=1}^{l} \hat{\zeta}_{i,w} f_{i,w}(\mathbf{x}_i) + r_{di}^{(n_i)} + \varepsilon_i \mathrm{sgn}(\mathbf{e}_i^{\mathrm{T}} P_i \mathbf{b}_i^{\mathrm{T}}) \tag{48}$$

$$\dot{\hat{\zeta}}_{i,w} = -\gamma_{\zeta i} f_{i,w} \mathbf{e}_i^{\mathrm{T}} P_i \mathbf{b}_i^{\mathrm{T}} \tag{49}$$

$$\dot{\hat{\eta}}_i = -\gamma_{\eta i} \frac{\mathbf{e}_i^{\mathrm{T}} P_i \mathbf{b}_i^{\mathrm{T}} \nu_i}{\hat{\eta}_i}, \quad (i = 1, 2) \tag{50}$$

For the neuro-adaptive scheme, the basis functions are chosen as

$$\psi_{b_{i,q}} = \exp\left(-\frac{\|\mathbf{z}_i - \zeta_{b_{i,q}}\|^2}{\sigma_{b_{i,q}}^2} \right) \tag{51}$$

$$\psi_{c_{i,q}} = \exp\left(-\frac{|\mathbf{e}_i^{\mathrm{T}} P_i \mathbf{b}_i - \zeta_{c_{i,q}}|^2}{\sigma_{c_{i,q}}^2} \right) \tag{52}$$

where $\mathbf{z}_i = [z_{3m+1}, z_{3m+2}, v_i]^{\mathrm{T}}$ as $m = i - 1$ based on Eqs. (10)–(15), and $\zeta_{b_{i,q}}$ and $\zeta_{c_{i,q}}$ indicate the centers of the influences of the basis functions defined as $\zeta_{b_{i,q}} = [\zeta_{b_{i,q1}}, \zeta_{b_{i,q2}}, \zeta_{b_{i,q3}}]^{\mathrm{T}}$ and $\zeta_{c_{i,q}} = [\zeta_{c_{i,q1}}, \zeta_{c_{i,q2}}, \zeta_{c_{i,q3}}]^{\mathrm{T}}$, respectively; here $i = 1$, 2 and we select the radial basis neural network nodes as $q = 1, \ldots, 200$. The $\sigma_{b_{i,q}}$ and $\sigma_{c_{i,q}}$ stand for the sizes of the influences of the basis functions which we select as $\sigma_{b_{i,q}} = \sigma_{c_{i,q}} = 0.1$. Note that we select the $u_{i,k}(\mathbf{z}_i)$ as a simple decentralized PI controller, $\Gamma_{b_i} = \Gamma_{c_i} = 10^3$, $\gamma_{\zeta_i} = \gamma_{\Omega_i} = 10^{-3}$, $f_i^L = 0.5$, and the Q_i and Hurwitz A_i matrices as

$$Q_i = \begin{bmatrix} q_i & 0 \\ 0 & q_i \end{bmatrix} \tag{53}$$

$$A_i = \begin{bmatrix} 0 & 1 \\ \underbrace{-1}_{a_{i,0}} & -\underbrace{7 \times 10^7}_{a_{i,1}} \end{bmatrix} \tag{54}$$

where $q_i = 1$ and $q_i = 8$ for the coupled chaotic and hyperchaotic dynamics, respectively. We also replaced the sign function of Eq. (37) with $\tanh(K \mathbf{e}_i^{\mathrm{T}} P_i \mathbf{b}_i)$ to avoid discontinuities expected in addition to guaranteeing uniqueness of the solution. We have implemented the decentralized neuro-adaptive formulations in MATLAB to be compared with the direct decentralized adaptive one with respect to the computational cost, practical feasibility, and robustness issues.

4 Results

Shown in Figs. 5 and 6 are the estimation processes for both the decentralized neuro- and direct-adaptive schemes suppressing the coupled chaotic dynamics. Comparing the results of both the schemes reveals the lack of robustness against uncertainties although the neuro-adaptive method seems to have slightly better performance than the direct-based one. In particular, the estimation process for the η_i's of the direct-based method (Fig. 6(*c*)), by revealing oscillatory-like profiles and also used in Eq. (47), would potentially result in practically infeasible control inputs.

It is of a great interest to observe that both the methods suppressing the coupled hyperchaotic dynamics timely converge. Figure 7 indicates that the neuro-adaptive scheme suppressing the coupled hyperchaos is considerably more robust than the chaotic case (Fig. 5). This looks interesting as the hyperchaotic network is subject to higher amplitude stochastic oscillations in comparison with the chaotic one (Fig. 3), and therefore, we expected to observe the better robustness for the neuro-adaptive scheme

Downloaded From: http://computationalnonlinear.asmedigitalcollection.asme.org/ on 04/03/2018 Terms of Use: http://www.asme.org/about-asme/terms-of-use

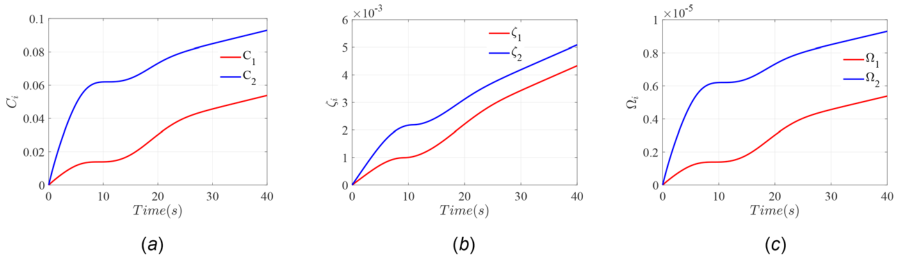

Fig. 5 The estimation process for the decentralized neuro-adaptive scheme suppressing the coupled chaotic dynamics; the lower and upper lines stand for the upstream and downstream agents

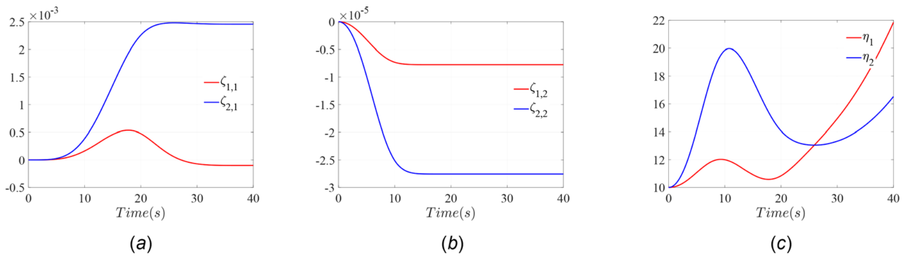

Fig. 6 The direct decentralized adaptive scheme's parameter estimation for sample $\zeta_{i,w}$ and η_i of both the upstream and downstream agents; (*a*) and (*c*): the lower and upper lines stand for the upstream and downstream agents and (*b*): the lower and upper lines indicate the downstream and upstream agents

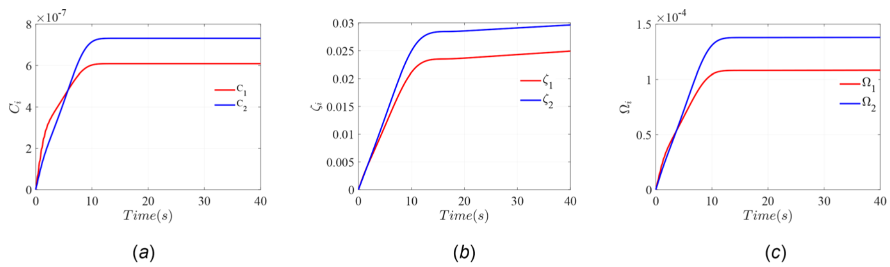

Fig. 7 The estimation process for the decentralized neuro-adaptive scheme suppressing the coupled hyperchaotic dynamics; the lower and upper lines stand for the upstream and downstream agents

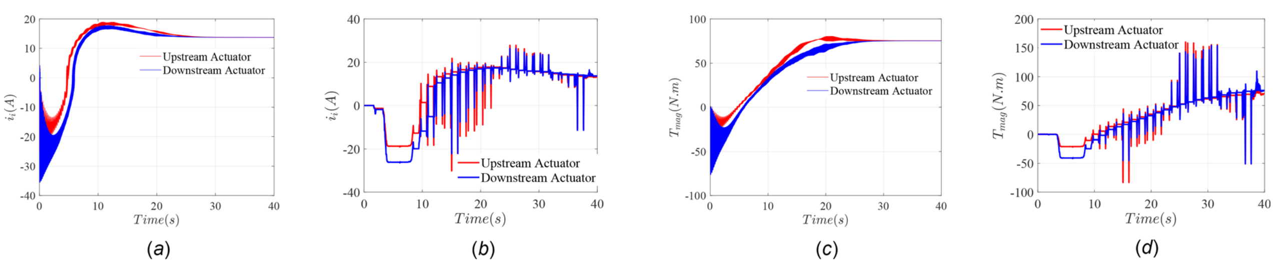

Fig. 8 (*a*) The neuro-adaptive control inputs, (*b*) the direct-based control inputs, (*c*) the neuro-adaptive magnetic torques, and (*d*) the direct-based magnetic torques

extinguishing the coupled chaotic dynamics. We also revealed [11] better robustness for the direct decentralized method suppressing the coupled hyperchaotic dynamics in comparison with the interconnected chaos. Therefore, selecting a superior performance for the robustness against uncertainties, as the first trade-off addressed earlier, between the decentralized neuro- and direct-adaptive methods looks challenging. However, it is obvious that the robustness of the centralized adaptive scheme, which we reported in Refs. [1] and [11], is significantly better than both the decentralized methods. Note that both the decentralized approaches, based on the "sufficient richness" condition [59,60], would not exactly estimate the unknown parameters such that the schemes expectedly yield values to allow the desired task to be carried out.

Shown in Fig. 8 are the control inputs and driving magnetic torques of both the neuro-adaptive and direct-based methods for the network subject to the coupled chaotic dynamics. By comparing Figs. 8(*a*) and 8(*b*), one can easily conclude that the neuro-adaptive control inputs are practically feasible in comparison with the chattering control inputs of the direct-based scheme. The same profiles of the control inputs are expected to be observed for the driving magnetic torques shown in Figs. 8(*c*) and 8(*d*). It is fairly

Downloaded From: http://computationalnonlinear.asmedigitalcollection.asme.org/ on 04/03/2018 Terms of Use: http://www.asme.org/about-asme/terms-of-use

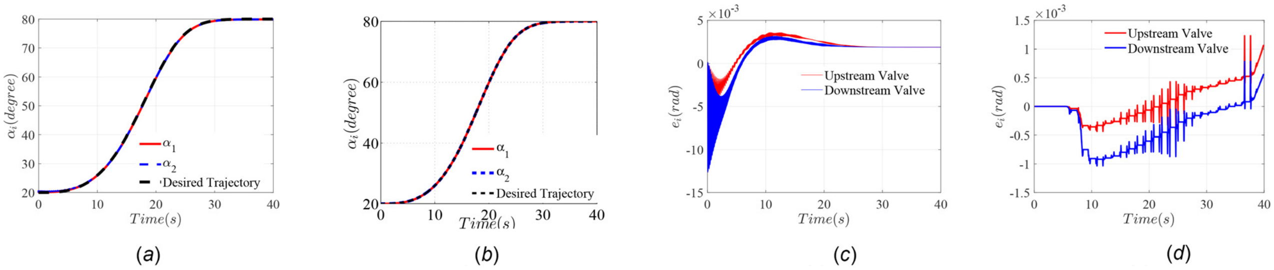

Fig. 9 (*a*) The neuro-adaptive valves' rotation angles, (*b*) the direct-based valves' rotation angles, (*c*) the neuro-adaptive error signals, and (*d*) the direct-based error signals

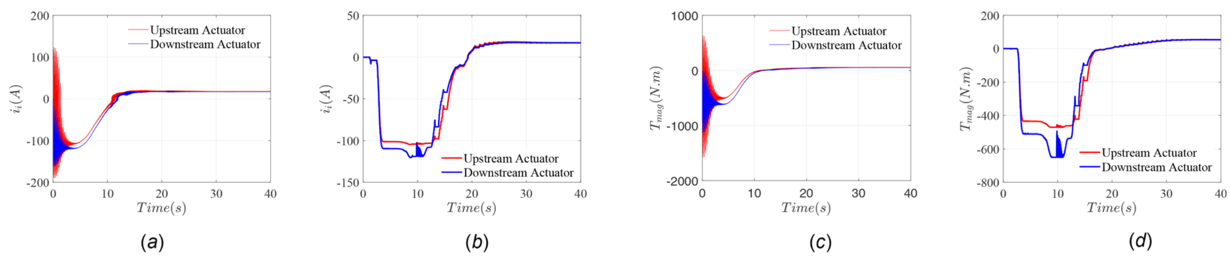

Fig. 10 (*a*) The neuro-adaptive control inputs, (*b*) the direct-based control inputs, (*c*) the neuro-adaptive magnetic torques, and (*d*) the direct-based magnetic torques

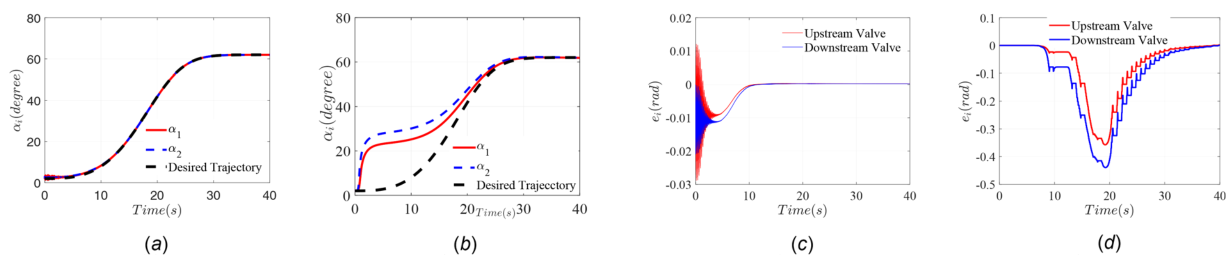

Fig. 11 (*a*) The neuro-adaptive valves' rotation angles, (*b*) the direct-based valves' rotation angles, (*c*) the neuro-adaptive error signals, and (*d*) the direct-based error signals

straightforward to conclude that implementing the control inputs and subsequently driving magnetic torques of the direct-based method in extinguishing the coupled chaotic dynamics would potentially result in failures of the coupled actuation units and gradually the whole network. Therefore, the neuro-adaptive scheme looks as a feasible tool for stabilizing the coupled chaotic network although another trade-off, the computational burden, needs to be carefully addressed.

Figure 9 presents the valves' rotation angles and tracking errors of both the schemes used in suppressing the coupled chaos. Figures 9(*a*) and 9(*b*) reveal that the upstream and downstream valves utilizing both the methods tend to the desirable trajectories (Eq. (21)). The tracking errors of the neuro-adaptive and direct-based methods presented in Figs. 9(*c*) and 9(*d*), respectively, are negligible although the direct-based scheme shows a better performance by yielding considerably smaller tracking errors in comparison with those of the neuro-adaptive one. Note that the noisy profiles of the direct-based tracking errors look logical with respect to the chattering control inputs. Considering the practically feasible control inputs of the neuro-adaptive method and its slightly better performance, with respect to the tracking errors of the direct-based one, we may select the neuro-adaptive scheme as an efficient and powerful controller to be used in suppressing the coupled chaotic dynamics. However, this selection would be questionable with respect to both the methods' computational times. The computation time of the direct-based scheme is one-fiftieth of the neuro-adaptive one: $t_{\text{direct}} = 0.867$ s and $t_{\text{neuro}} = 40$ s. Therefore, using the neuro-adaptive method would potentially cause crucial issues by adding more agents into the network. Consequently, an important trade-off needs to be addressed between the practical feasibility of control inputs and computational burden for extinguishing the interconnected chaotic dynamics.

Shown in Fig. 10 are the control inputs and driving magnetic torques to be used in suppressing the coupled hyperchaotic dynamics of two agents. As expected, higher control inputs and subsequently driving magnetic torques, for both the schemes, need to be applied in order to extinguish the coupled hyperchaos in comparison with the interconnected chaotic dynamics (Fig. 8). This looks logical with respect to the larger domains of attractions of the hyperchaotic responses than those of the chaotic ones. It is of a great interest to observe that the control inputs of both the schemes (Figs. 10(*a*) and 10(*b*)), in the presence of the hyperchaotic responses having the higher amplitude stochastic oscillations, are almost practically feasible. However, the neuro-based method yields slightly smoother control inputs, except within small transient domains limited up to 3 s, than those of the direct-based one. The same profiles are logically expected to be observed for the driving magnetic torques shown in Figs. 10(*c*) and 10(*d*). Therefore, the practical feasibility of control inputs would not be a critical issue for selecting between the neuro-adaptive and direct-based methods. Hence, the other trade-offs need to be carefully considered.

Figure 11 presents the valves' rotation angles and tracking errors of both the neuro-adaptive and direct-based schemes utilized in suppressing the coupled hyperchaos. Despite the agents' motions subject to the coupled chaotic dynamics (Figs. 9(*a*) and

Downloaded From: http://computationalnonlinear.asmedigitalcollection.asme.org/ on 04/03/2018 Terms of Use: http://www.asme.org/about-asme/terms-of-use

9(b)), we are able to distinguish considerable differences for the valves' rotation angles shown in Figs. 11(a) and 11(b). It is fairly straightforward to conclude that the neuro-adaptive scheme outperforms the direct-based one for perfect tracking of the desirable trajectories (Eq. (22)). Although both the valves, using the direct-based scheme, finally reach to the angles targeted ($\alpha_{di_f} = 62$ deg), the direct-based method is inefficient for wide ranges of the transient responses, as shown in Fig. 11(b). We hence expect to observe significant higher tracking errors for both the agents controlled by the direct-based scheme than those of the neuro-adaptive one (Figs. 11(c) and 11(d)). It is interesting to note that, despite the network subject to the coupled chaotic dynamics, the tracking errors of both the agents using the neuro-adaptive scheme converge almost to zero; we expected to observe the convergence of tracking errors to zero for the network subject to the coupled chaos.

The smoother control inputs, except within the small transient domains, in addition to the convergence of tracking errors to zero for the neuro-adaptive scheme extinguishing the coupled hyperchaos lead us to an easy selection between the methods. However, the computation time of the neuro-adaptive scheme is higher than that of the direct-based one for when the two agents are subject to the coupled hyperchaos: $t_{\text{direct}} = 0.981$ s and $t_{\text{neuro}} = 45.34$ s. We hence need to address the important trade-offs which include the smoother control inputs and smaller tracking errors of the neuro-adaptive and considerable lower computation time of the direct-based methods for suppressing the interconnected hyperchaotic dynamics.

5 Conclusions

Through this comparative research effort, we first represented the sixth-order interconnected analytical model of two bidirectional solenoid actuated butterfly valves operating in series. The initial conditions along with the critical parameters leading to the coupled chaotic and hyperchaotic dynamics were presented to be used in generating the energy-efficient desirable trajectories. The harmful responses were then characterized using the powerful tools of Lyapunov exponents and Poincaré map. We could reveal the coupled chaos and hyperchaos with the aid of one and two positive Lyapunov exponents, respectively, along with the irregular Poincaré maps of the two agents. We utilized both the decentralized neuro- and direct-adaptive schemes for extinguishing both the coupled chaotic and hyperchaotic dynamics.

It was shown that, for the coupled chaos, the neuro-adaptive scheme yields practically feasible control inputs and subsequently the driving magnetic torques; the direct-based method leads to the chattering control inputs. Although the second trade-off, the computation time, can be helpful to properly select between the methods. Note that the computation time of the direct-based method is one-fiftieth of the neuro-adaptive one only for the two agents.

Surprisingly, the control inputs and subsequently the driving magnetic torques of both the methods suppressing the coupled hyperchaos are almost practically feasible; the neuro-adaptive method yields slightly smoother control inputs, except within the small transient domains, in comparison with the direct-based scheme. Also, the tracking errors of the neuro-adaptive scheme converge almost to zero, which may potentially outperform the direct-based method. However, the computational cost of the neuro-adaptive method is higher than that of the direct-based one.

References

[1] Naseradinmousavi, P., Ashrafiuon, H., and Ayoubi, M. A., 2018, "An Adaptive Centralized Approach to Control Chaotic and Hyperchaotic Dynamics of Smart Valves Network," ASME J. Comput. Nonlinear Dyn., **13**(1), p. 011002.

[2] Naseradinmousavi, P., Segala, D. B., and Nataraj, C., 2016, "Chaotic and Hyperchaotic Dynamics of Smart Valves System Subject to a Sudden Contraction," ASME J. Comput. Nonlinear Dyn., **11**(5), p. 051025.

[3] Naseradinmousavi, P., Krstic, M., and Nataraj, C., 2016, "Design Optimization of Dynamically Coupled Actuated Butterfly Valves Subject to a Sudden Contraction," ASME J. Mech. Des., **138**(4), p. 041402.

[4] Naseradinmousavi, P., Machiani, S. G., Ayoubi, M. A., and Nataraj, C., 2017, "Coupled Operational Optimization of Smart Valve System Subject to Different Approach Angles of a Pipe Contraction," J. Struct. Multidiscip. Optim., **55**(3), pp. 1001–1015.

[5] Naseradinmousavi, P., 2014, "A Novel Nonlinear Modeling and Dynamic Analysis of Solenoid Actuated Butterfly Valves Coupled in Series," ASME J. Dyn. Syst. Meas. Control, **137**(1), p. 014505.

[6] Naseradinmousavi, P., and Nataraj, C., 2013, "Optimal Design of Solenoid Actuators Driving Butterfly Valves," ASME J. Mech. Des., **135**(9), p. 094501.

[7] Naseradinmousavi, P., and Nataraj, C., 2012, "Transient Chaos and Crisis Phenomena in Butterfly Valves Driven by Solenoid Actuators," J. Commun. Nonlinear Sci. Numer. Simul., **17**(11), pp. 4336–4345.

[8] Lee, D., Naseradinmousavi, P., and Nataraj, C., 2012, "Nonlinear Model-Based Adaptive Control of a Solenoid-Valve System," J. Control Sci. Eng., **2012**, p. 846458.

[9] Naseradinmousavi, P., and Nataraj, C., 2011, "Nonlinear Mathematical Modeling of Butterfly Valves Driven by Solenoid Actuators," J. Appl. Math. Model., **35**(5), pp. 2324–2335.

[10] Naseradinmousavi, P., Ashrafiuon, H., and Bagheri, M., 2018, "Suppressing Chaotic and Hyperchaotic Dynamics of Smart Valves Network Using a Centralized Adaptive Approach," American Control Conference (ACC), Milwaukee, WI, June 27–29, Paper No. 1056.

[11] Naseradinmousavi, P., Bagheri, M., Ashrafiuon, H., Canova, M., and Segala, D. B., 2017, "Suppressing Chaotic/Hyperchaotic Dynamics of Smart Valves Network Using Decentralized and Centralized Schemes," ASME Paper No. DSCC2017-5006.

[12] Naseradinmousavi, P., Krstic, M., Bagheri, M., and Nataraj, C., 2016, "Coupled Chaotic and Hyperchaotic Dynamics of Actuated Butterfly Valves Operating in Series," ASME Paper No. DSCC2016-9601.

[13] Naseradinmousavi, P., Bagheri, M., and Nataraj, C., 2016, "Coupled Operational Optimization of Smart Valve System Subject to Different Approach Angles of a Pipe Contraction," ASME Paper No. DSCC2016-9627.

[14] Naseradinmousavi, P., and Nataraj, C., 2015, "Design Optimization of Solenoid Actuated Butterfly Valves Dynamically Coupled in Series," ASME Paper No. DSCC2015-9605.

[15] Naseradinmousavi, P., 2015, "Optimal Design of Solenoid Actuated Butterfly Valves Dynamically Coupled in Series," ASME Paper No. IMECE2015-50094.

[16] Naseradinmousavi, P., and Nataraj, C., 2011, "A Chaotic Blue Sky Catastrophe of Butterfly Valves Driven by Solenoid Actuators," ASME Paper No. IMECE2011-62608.

[17] Zhang, X., and Liao, L., 2016, "Compound Synchronization Based on Memristive Cellular Neural Network of Chaos System," ASME J. Comput. Nonlinear Dyn., **12**(3), p. 031002.

[18] Chang-Jian, C.-W., 2014, "Gear Dynamics Analysis With Turbulent Journal Bearings Mounted Hybrid Squeeze Film Damper-Chaos and Active Control Analysis," ASME J. Comput. Nonlinear Dyn., **10**(1), p. 011011.

[19] Morel, C., Vlad, R., and Morel, J.-Y., 2008, "Anticontrol of Chaos Reduces Spectral Emissions," ASME J. Comput. Nonlinear Dyn., **3**(4), p. 041009.

[20] Luo, R., and Zeng, Y., 2016, "The Control and Synchronization of a Class of Chaotic Systems With Output Variable and External Disturbance," ASME J. Comput. Nonlinear Dyn., **11**(5), p. 051011.

[21] Lin, C.-H., 2015, "Application of v-Belt Continuously Variable Transmission System Using Hybrid Recurrent Laguerre Orthogonal Polynomials Neural Network Control System and Modified Particle Swarm Optimization," ASME J. Comput. Nonlinear Dyn., **10**(5), p. 051019.

[22] Reddy, B. S., and Ghosal, A., 2016, "Asymptotic Stability and Chaotic Motions in Trajectory Following Feedback Controlled Robots," ASME J. Comput. Nonlinear Dyn., **11**(5), p. 051012.

[23] Khamsuwan, P., and Kuntanapreeda, S., 2016, "A Linear Matrix Inequality Approach to Output Feedback Control of Fractional-Order Unified Chaotic Systems With One Control Input," ASME J. Comput. Nonlinear Dyn., **11**(5), p. 051021.

[24] Merat, K., Chekan, J. A., Salarieh, H., and Alasty, A., 2014, "Control of Discrete Time Chaotic Systems Via Combination of Linear and Nonlinear Dynamic Programming," ASME J. Comput. Nonlinear Dyn., **10**(1), p. 011008.

[25] Tian, X., and Fei, S., 2015, "Adaptive Control for Fractional-Order Micro-Electro-Mechanical Resonator With Nonsymmetric Dead-Zone Input," ASME J. Comput. Nonlinear Dyn., **10**(6), p. 061022.

[26] Arefi, M. M., 2016, "Adaptive Robust Stabilization of Rossler System With Time-Varying Mismatched Parameters Via Scalar Input," ASME J. Comput. Nonlinear Dyn., **11**(4), p. 041024.

[27] Chen, D., and Liu, W., 2016, "Chaotic Behavior and Its Control in a Fractional-Order Energy Demand-Supply System," ASME J. Comput. Nonlinear Dyn., **11**(6), p. 061010.

[28] Chen, X., Cao, J., Qiu, J., Alsaedi, A., and Alsaadi, F. E., 2016, "Adaptive Control of Multiple Chaotic Systems With Unknown Parameters in Two Different Synchronization Modes," *Advances in Difference Equations*, Springer, New York, p. 231.

[29] Zomaya, A. Y., and Nabhan, T. M., 1993, "Centralized and Decentralized Neuro-Adaptive Robot Controllers," Neural Networks, **6**(2), pp. 223–244.

[30] Chen, Y. H., 1991, "Decentralized Adaptive Robust Control Design: The Uncertainty is Time Varying," ASME J. Dyn. Syst. Meas. Control, **113**(3), pp. 515–518.

[31] Hsiao, F.-H., Liang, Y.-W., Xu, S.-D., and Lee, G.-C., 2005, "Decentralized Stabilization of Neural Network Linearly Interconnected Systems Via t-s Fuzzy Control," ASME J. Dyn. Syst. Meas. Control, **129**(3), pp. 343–351.

[32] Karpenko, M., Sepehri, N., and Anderson, J., 2007, "Decentralized Coordinated Motion Control of Two Hydraulic Actuators Handling a Common Object," ASME J. Dyn. Syst. Meas. Control, **129**(5), pp. 729–741.

Downloaded From: http://computationalnonlinear.asmedigitalcollection.asme.org/ on 04/03/2018 Terms of Use: http://www.asme.org/about-asme/terms-of-use

[33] Yang, Y., and Yue, D., 2017, "Observer-Based Decentralized Adaptive NNs Fault-Tolerant Control of a Class of Large-Scale Uncertain Nonlinear Systems With Actuator Failures," IEEE Trans. Syst., Man, Cybern. Syst., **PP**(99), pp. 1–15.
[34] Eltantawie, M. A., 2012, "Decentralized Neuro-Fuzzy Control for Half Car With Semi-Active Suspension System," Int. J. Automot. Technol., **13**(3), pp. 423–431.
[35] Shi, L., and Singh, S. K., 1992, "Decentralized Adaptive Controller Design for Large-Scale Systems With Higher-Order Interconnections," American Control Conference (ACC), Chicago, IL, June 24–26, pp. 3146–3150.
[36] Duan, N., and Min, H.-F., 2016, "Decentralized Adaptive NN State-Feedback Control for Large-Scale Stochastic High-Order Nonlinear Systems," J. Neurocomput., **173**, pp. 1412–1421.
[37] Tong, S., Li, Y., and Wang, T., 2013, "Adaptive Fuzzy Decentralized Output Feedback Control for Stochastic Nonlinear Large-Scale Systems Using DSC Technique," Int. J. Robust Nonlinear Control, **23**(4), pp. 381–399.
[38] Zhang, X., Ma, H., and Yang, C., 2017, "Decentralized Adaptive Control of a Class of Hidden Leader-Follower Nonlinearly Parameterized Coupled Multi-Agent Systems," IET Control Theory Appl., **11**(17), pp. 3016–3025.
[39] Skworcow, P., Ulanicki, B., AbdelMeguid, H., and Paluszczyszyn, D., 2010, "Model Predictive Control for Energy and Leakage Management in Water Distribution Systems," UKACC Eighth International Conference on Control, Coventry, UK, Sept. 7–10, pp. 990–995.
[40] Negenborn, R., Schutter, B. D., and Hellendoorn, J., 2008, "Multi-Agent Model Predictive Control for Transportation Networks: Serial Vs. parallel Schemes," Eng. Appl. Artif. Intell., **21**(3), pp. 353–366.
[41] Bottura, C. P., and Caceres, A. F. T., 2002, "Decentralized Control of Serial Interconnected Systems for River Water Quality Via Subspace Identification," American Control Conference (ACC), Anchorage, AK, May 8–10, pp. 3338–3342.
[42] Joseph-Duran, B., Ocampo-Martinez, C., and Cembrano, G., 2015, "Output-Feedback Control of Combined Sewer Networks Through Receding Horizon Control With Moving Horizon Estimation," Water Resour. Res., **51**(10), pp. 8129–8145.
[43] Grosso, J. M., Velarde, P., Ocampo-Martinez, C., Maestre, J. M., and Puig, V., 2016, "Stochastic Model Predictive Control Approaches Applied to Drinking Water Networks," Optim. Control Appl. Methods, **38**(4), pp. 541–588.
[44] Fambrini, V., and Ocampo-Martinez, C., 2009, "Modelling and Decentralized Model Predictive Control of Drinking Water Networks," Institut de Robotica i Informatica Industrial (CSIC-UPC), Barcelona, Spain, Technical Report No. IRI-TR-04-09.
[45] Barcelli, D., Ocampo-Martinez, C., Puig, V., and Bemporad, A., 2010, "Decentralized Model Predictive Control of Drinking Water Networks Using an Automatic Subsystem Decomposition Approach," IFAC Proc. Vol., **43**(8), pp. 572–577.
[46] Park, J. Y., and Chung, M. K., 2006, "Study on Hydrodynamic Torque of a Butterfly Valve," ASME J. Fluids Eng., **128**(1), pp. 190–195.
[47] Naseradinmousavi, P., 2012, "Nonlinear Modeling, Dynamic Analysis, and Optimal Design and Operation of Electromechanical Valve Systems," Ph.D. thesis, Villanova University, Villanova, PA.
[48] Bennett, C. O., and Myers, J. E., 1962, *Momentum, Heat, and Mass Transfer*, McGraw-Hill, New York.
[49] Massey, B. S., and Ward-Smith, J., 1998, *Mechanics of Fluids*, 7th ed., Taylor & Francis, Boca Raton, FL.
[50] Khalil, H. K., 2002, *Nonlinear Systems*, Prentice Hall, Upper Saddle River, NJ.
[51] Wolf, A., Swift, J. B., Swinney, H. L., and Vastano, J. A., 1985, "Determining Lyapunov Exponents From a Time Series," Phys. D, **16**(3), pp. 285–317.
[52] Karimi, B., Menhaj, M. B., Karmi-Ghartemani, M., and Saboori, I., 2009, "Decentralized Adaptie Control of Large-Scale Affine and Nonaffine Nonlinear Systems," IEEE Trans. Instrum. Meas., **58**(8), pp. 2459–2467.
[53] Spooner, J. T., and Passino, K. M., 1996, "Adaptive Control of a Class of Decentralized Nonlinear Systems," IEEE Trans. Autom. Control, **41**(2), pp. 280–284.
[54] Wen, C., 1995, "Indirect Robust Totally Decentralized Adaptive Control of Continuous-Time Interconnected Systems," IEEE Trans. Autom. Control, **40**(6), pp. 1122–1126.
[55] Wen, C., 1994, "Direct Decentralized Adaptive Control of Interconnected Systems Having Arbitrary Subsystem Relative Degrees," 33rd IEEE Conference on Decision and Control (CDC), Lake Buena Vista, FL, Dec. 14–16, pp. 1187–1192.
[56] Lang, S., 1983, *Real Analysis*, Addison-Wesley, Boston, MA.
[57] Karimi, B., Menhaj, M. B., Karmi-Ghartemani, M., and Saboori, I., 2007, "A Decentralized Direct Adaptive Controller for a Class of Large-Scale Interconnected Nonlinear Systems," IEEE International Symposium on Intelligent Signal Processing (WISP), Alcala de Henares, Spain, Oct. 3–5, pp. 265–270.
[58] Karimi, B., Menhaj, M. B., and Saboori, I., 2007, "Decentralized Adaptive Control of Large-Scale Nonaffine Nonlinear Systems Using Radial Basis Function Neural Networks," IEICE Trans. Fundam., **E90-A**(10), pp. 2239–2247.
[59] Krstić, M., Kanellakopoulos, I., and Kokotović, P., 1995, *Nonlinear and Adaptive Control Design*, Wiley-Interscience, New York.
[60] Slotine, J. J. E., and Li, W., 1991, *Applied Nonlinear Control*, Prentice Hall, Upper Saddle River, NJ.

Downloaded From: http://computationalnonlinear.asmedigitalcollection.asme.org/ on 04/03/2018 Terms of Use: http://www.asme.org/about-asme/terms-of-use